Miniature Long-Range Ceramic On-Metal RFID Tag

Ildar Yusupov, *Member, IEEE*, Dmitry Dobrykh, *Graduate Student Member, IEEE*, Dmitry Filonov, *Member, IEEE*, Alexey Slobozhanyuk, *Member, IEEE*, and Pavel Ginzburg, *Member, IEEE*

***Abstract*— Radio frequency identification (RFID) is a widely used wireless technology for contactless data exchange between a passive information carrier (tag) and an active interrogation device (reader). Being sensitive to a surrounding environment, RFID tags are usually designed per application. Here, we demonstrate an RFID tag with three essential functions available simultaneously, namely, small footprint, long reading range, and capability of on-metal labeling. Our design is based on a compact high-index ceramic resonator and an inductively coupled small metal ring functionalized with an RFID chip. The tag operates at magnetic dipolar resonance, which interacts with the metal object subject to labeling. Specifically, a 16.5 mm × 16.5 mm × 12 mm footprint device, placed on a 40 cm × 40 cm metal sheet, was successfully interrogated from 22 m with no violation of international effective isotropic radiated power (EIRP) standards. Currently, it is the smallest on-metal RFID tag with a reading range of over 20 m. Multifunctional miniature long-range ceramic tags are attractive for use in numerous practical applications, including the Internet of *Small* Things (IoST) and many others.**

***Index Terms*— Ceramic resonators, dielectric resonant antennas (DRAs), on-metal RFID tags.**

I. Introduction

RADIO frequency identification (RFID) allows short-range wireless data exchange between multiple users. Apart from traditional applications in retail, personal identification, and billing systems, the well-established RFID technology can contribute to the new emerging trends in the Internet of Things [1]. In particular, extremely low-cost passive RFID tags can be considered consumables, which makes labeling small items affordable. Internet of *Small* Things (IoST) promotes the idea of a global network, in which small items become subject to identification and tracking. Apart from low cost, the main technical requirements for tags, in this case, are: 1) long reading range; 2) omnidirectional response; 3) small footprint; and 4) capability of object-independent labeling. While all those functions can be achieved separately [2]–[9], meeting all of the abovementioned requirements within a single device remains a challenge. Here, we present an RFID tag simultaneously demonstrating three functions: small footprint, long reading range, and a capability of on-metal labeling.

A passive RFID tag consists of an antenna and an integrated circuit (IC). The antenna harvests an interrogating signal, which is partially rectified to power the electronics. The IC modulates the antenna impedance, leading to time-modulated backscattering, which encodes the information stored in the tag memory. In the most cases, tag performance can be tailored per specific application by changing its antenna design. A typical tag antenna layout is based on a meandered electric dipole printed on a thin, flexible adhesive substrate. However, this design makes tags extremely sensitive to the surrounding environment, especially if there are metal objects located near the tag. In this case, special designs are required.

On-metal ultrahigh-frequency (UHF) RFID tags were developed for labeling containers transported by railways or by sea [10], [11]. Quite a few different approaches to on-metal tagging have been proposed and demonstrated. For example, dipole-like antennas with high-index dielectric substrates [12], microstrip patch antennas [13], [14], meandered patches [15], planar inverted-F antennas [16], and cavity-type antennas [17], [18] showed reliable performances. However, all these solutions must reach a compromise between the footprint and the reading range, as we summarized in the section with experimental results, quantitatively comparing our realization and other existing reports.

An antenna located in close proximity to a metal surface is a well-known and widely studied electromagnetic problem [19]. Nevertheless, demonstrating a compact on-metal antenna with high radiation efficiency remains challenging in many practical cases.

An electric dipole antenna radiates efficiently only if placed at a distance of quarter wavelength ($\lambda_0/4$ in free space) above the metal surface [see Fig. 1(a)]. In this case, the field

Manuscript received 21 December 2021; revised 7 July 2022; accepted 13 July 2022. Date of publication 8 August 2022; date of current version 17 November 2022. This work was supported by the Russian Science Foundation for Basic Research, Sirius University of Science and Technology, Joint-Stock Company (JSC) Russian Railways and Educational Fund "Talent and Success," under Project 20-37-51011. The work of Alexey Slobozhanyuk was supported by the Foundation for the Advancement of Theoretical Physics and Mathematics "BASIS." The work of Pavel Ginzburg was supported in part by the European Research Council (ERC) Starting Grants (StG) "In Motion" under Grant 802279, in part by the PAZY Foundation, and in part by the Israeli Ministry of Science and Technology through the Project "Integrated 2-D and 3-D Functional Printing of Batteries with Metamaterials and Antennas. *(Corresponding author: Ildar Yusupov.)*

Ildar Yusupov and Alexey Slobozhanyuk are with the School of Physics and Engineering, ITMO University, 197101 Saint Petersburg, Russia, and also with Sirius University, 354349 Sochi, Russia (e-mail: ildar.yusupov@metalab.ifmo.ru; a.slobozhanyuk@metalab.ifmo.ru).

Dmitry Dobrykh and Pavel Ginzburg are with the School of Electrical Engineering, Tel Aviv University, Tel Aviv 69978, Israel (e-mail: dmitryd@mail.tau.ac.il; pginzburg@post.tau.ac.il).

Dmitry Filonov is with the Center for Photonics and 2-D Materials, Moscow Institute of Physics and Technology, 141700 Dolgoprudny, Russia, and also with Sirius University, 354349 Sochi, Russia (e-mail: filonov.ds@mipt.ru).

Color versions of one or more figures in this article are available at https://doi.org/10.1109/TAP.2022.3195551.

Digital Object Identifier 10.1109/TAP.2022.3195551

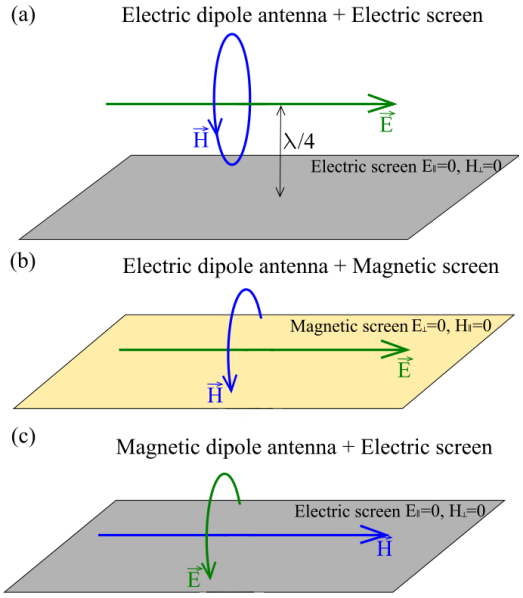

Fig. 1. Substrate–antenna interaction. (a) Electric dipole above the electric screen [perfect electric conductor (PEC)]. (b) Electric dipole above the magnetic screen (PMC). (c) Magnetic dipole above the PEC. In all the scenarios, the dipole moment is oriented parallel to the surface.

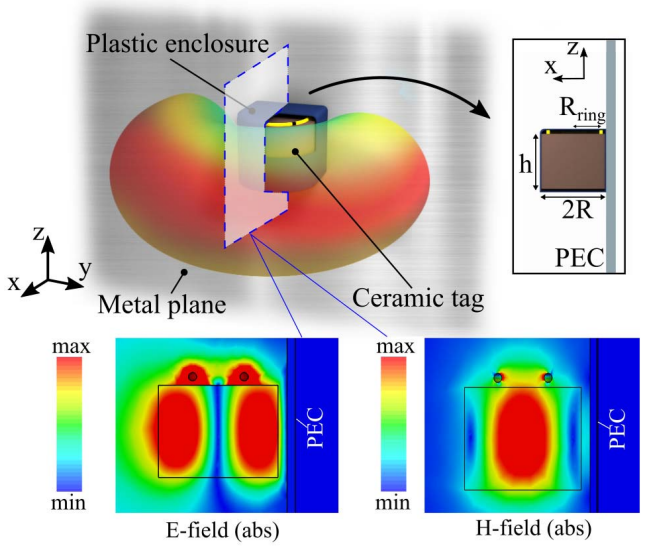

Fig. 2. Miniature long-range ceramic on-metal RFID tag. The tag consists of a cylindrical high-index ceramic resonator and a metallic split ring, functionalized with an RFID chip. The tag is encapsulated in a plastic holder and attached to a metal surface.

reflected from the surface comes in-phase with the antenna's current [20]. Otherwise, the radiation is quenched. A possible solution is a special magnetic screen [e.g., approaching the performance of a perfect magnetic conductor (PMC)] [see Fig. 1(b)], which allows placing an electric dipole antenna directly on a surface [21], [22]. However, practical realizations of magnetic screens are quite challenging, as they lead to bulky narrowband solutions. These aspects significantly limit the practical applications of RFID.

A conceptually different designs can be chosen, based on a magnetic dipole antenna attached to a metal screen [see Fig. 1(c)]. In this case, the magnetic dipole moment should be parallel to the surface; otherwise, the radiation will be quenched. However, practically realizable magnetic dipoles have a finite size, which means that retardation effects arise. A split ring with a normal parallel to the surface is a representative example. In this case, the reflected wave accumulates a phase over the ring's diameter, degrading the condition of a perfect constructive interference. We propose a high-index dielectric resonator as a solution to this problem. It operates at the fundamental TE_{010} (magnetic dipole) mode, which allows putting the structure directly on a metal surface. Owing to the high-index ceramic material, the overall footprint of the resonator is quite small, reducing the impact of the destructive interference.

Our on-metal tag architecture is based on a ceramic cylinder supporting a magnetic dipole mode (see Fig. 2). A miniature nonresonant metal split ring with a standard RFID chip soldered in the ring's gap is placed on top of the resonator. Since the main antenna element is a ceramic cylinder, an inductively coupled metal ring converts the displacement current in the dielectric into conduction currents, which drive the IC soldered in the metal split ring. A thin 3-D-printed plastic enclosure is an additional element. It has no electromagnetic function and serves as a protection layer, forming a geometry for convenient placement on metal (see Fig. 2).

We have recently developed a new architecture of long-range ceramic tags [8], which has proven to be beneficial in many applications relevant to IoST. However, we did not consider on-metal tagging, which requires different design rules, as we will discuss hereinafter. Specifically, the interplay between the form factor, permittivity, and the required retardation plays the key role.

II. Antenna Design

We chose the free-space tag that we have demonstrated in [8] as a starting point for optimization. This geometry has already proved itself tunable per application. This aspect is quite important from the technological point of view, as it paves a way for low-cost manufacturing. The main tag parameters to be optimized are the cylinder dimensions and its permittivity. The ceramic elements are provided by "Ceramics Ltd." [23], manufacturing a wide range of materials with tunable low-loss permittivity. Consequently, we can reduce the resonator footprint by increasing its refractive index [24]. However, the drawback of this approach is the bandwidth reduction of dipole channel, according to the Chu–Harrington limit (e.g., [25]–[27]). RFID communication protocol sets a lower bound on the bandwidth (250–500 kHz per single channel in the EPCGEN2 protocol). As a result of the size-permittivity tradeoff, we chose $\varepsilon_r = 506$ with $tan\,\delta = 4 \cdot 10^{-4}$. Other system parameters were optimized as follows: the cylinder dimensions were chosen to support a resonance near 865–868 MHz (Europe UHF RFID band).

We achieved the impedance matching conditions between the chip and the tag antenna (the resonator and the ring)

TABLE I
POSSIBLE PARAMETERS OF METAL-MOUNTABLE RFID TAGS

Radius R, mm	Height h, mm	R/h	Resonator's volume, mm^3
7.7	9	0.855	1676
7.5	9.9	0.758	1750
7.3	11	0.663	1842
7	13.55	0.516	2086
6.8	15.8	0.431	2296

by adjusting the inductive coupling coefficient between the ring and the resonator. Control over the relative geometric arrangement allows matching and, furthermore, tuning the operational frequency. This parameter can be changed by varying the radius and thickness of the ring and its position above the resonator [24]. In the experiment, the resonant frequency of the tag is tuned by shifting the ring with respect to the center of the cylinder. The ratio between the cylinder radius and height (R/h) can also be optimized to reduce the tag footprint. As the cylinder's axis is parallel to the metal plane, the radius dictates the profile above the surface. Table I summarizes the tag parameters, given that the resonant frequency of TE_{010} mode and the cylinder permittivity are fixed. Reducing the radius cause to a fat growth of the height and, consequently, the volume of the resonator. Considering the above, we found $R/h \sim 0.5$–0.7 to be an empirical optimum. The chosen set of parameters is highlighted in Table I with green color.

We chose the following final design: a ceramic resonator with a small conductive ring is placed at a distance of 1 mm above the metal surface. This distance corresponds to the width of the plastic holder in the forthcoming experiment. The resonator parameters are: radius $R = 7.3$ mm, height $h = 11$ mm, and permittivity $\varepsilon_r = 506$ with $tan\,\delta = 4 \cdot 10^{-4}$. The radius of the nonresonant metal split ring made of a thin copper wire is $R_{ring} = 3.2$ mm. These parameters correspond to the resonant frequency of the on-metal tag equal to 868 MHz.

For proper operation of the tag, the impedances of the antenna and the IC should be matched. A usual analysis tool is an equivalent circuit model. In case of a distributed system such as ours, nominal values are not known, and the parameters can be retrieved in a limited set of measurements. Thus, we connected a vector network analyzer (Rohde and Schwarz ZVB20) into the ring's gap instead of the RFID IC. Fig. 3 shows the real and imaginary parts of the impedance as a function of frequency. Dashed-dotted purple lines are the complex conjugate impedance of chip (one of its states) taken from the vendor's IC's datasheet (Impinj Monza R6). The conjugate matching is obtained at 867.8 MHz, where antenna impedance is $Z_{exp} = 12.7 - 147.8j$ (experiment). The numerical modeling values are 868.4 MHz and $Z_{num} = 11.3 - 147.6j$. The metal screen dimensions are 40 cm $\times$ 40 cm.

Based on this experimental information, an equivalent scheme is proposed [see Fig. 3(c)]. It consists of three inductively coupled circuits, namely: 1) R_r, L_r, and C_r of the metal ring; 2) R_d, L_d, and C_d of the ceramic resonator; and 3) resonator's image in the metal screen. For simplicity, we assumed that the ceramic resonator and its image have equal parameters. Mutual inductances, M_1 and M_2, appear on the scheme. Coupling between the metal ring and the screen plays a secondary role, and it was neglected. As the system operates primarily on a magnetic mode, we used inductive couplings.

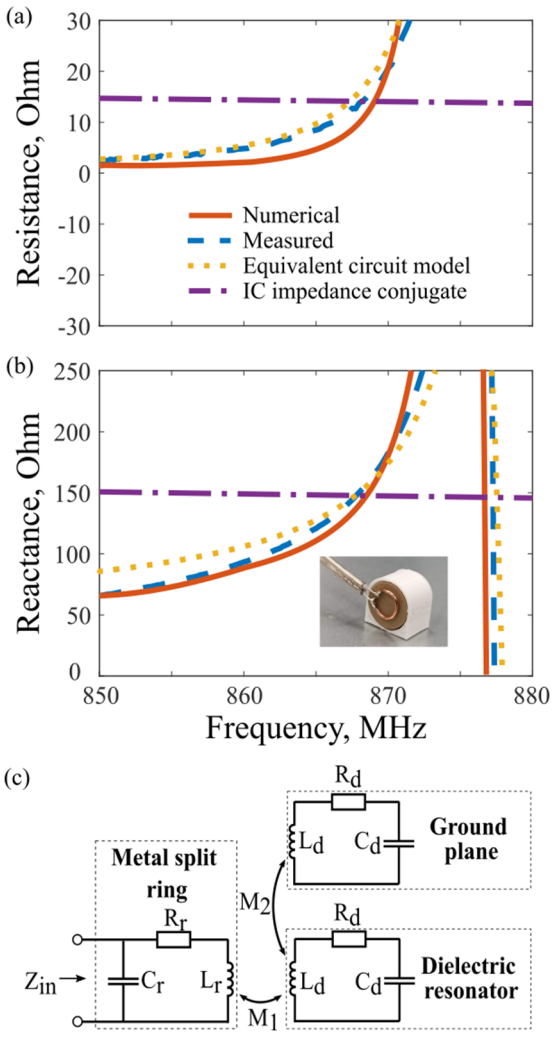

Fig. 3. (a) Real and (b) imaginary parts of the input impedance as a function of frequency. Red solid lines are the numerical calculations in CST, blue dashed lines mark experimental data, orange dotted lines are the equivalent circuit fit, and the purple dashed-dotted lines are the complex conjugate of the tag's IC (Impinj Monza R6). Photograph of the experimental design used to measure the impedance (inset). (c) Equivalent circuit of the tag on metal.

The parameters of the system [see Fig. 3(c)] were retrieved with the models reported in [28] and [29], where a cylindrical resonator was fed with a strip line. The input impedance of the system (the port is connected to the ring's gap) can be found as [30]

$$Z_{in} = 1 \Big/ \left[\frac{Z_1 + Z_2}{Z_1 Z_2 + Z_3(Z_1 + Z_2)} + \frac{1}{Z_4} \right] \tag{1}$$

TABLE II
PARAMETERS OF THE EQUIVALENT CIRCUIT

R_r Ohm	R_d Ohm	L_r nH	L_d nH	C_r pF	C_d pF	M_1 nH	M_2 nH
0.88	0.08	12.17	4.38	0.045	7.80	3.3	1.39

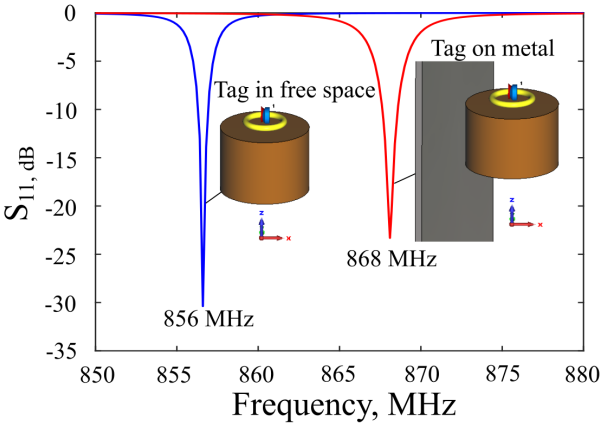

Fig. 4. Numerically calculated $|S_{11}|$ spectra of the ceramic tag in free space and on the 40 cm × 40 cm metal surface. Models of a ceramic RFID tag (inset).

where

$$Z_1 = j\omega(L_d - M_1 - M_2) + \frac{1}{Z_1'}$$
$$Z_1' = \frac{1}{R_d - 1/j\omega C_d} + \frac{1}{j\omega M_2} + \frac{1}{R_d + 1/j\omega C_d + j\omega(L_d - M_2)}$$
$$Z_2 = j\omega M_1$$
$$Z_3 = R_r + j\omega(L_r - M_1)$$
$$Z_4 = 1/j\omega C_r.$$

The nominals can be found by comparing (1) to the experimental data. Yellow dotted line in Fig. 3 shows the results. It is worth noting that the equivalent scheme is not unique, and different representations can be found. The retrieved parameters are summarized in Table II.

Next, we will study the radiation patterns tailored by metal substrate to verify the low sensitivity of on-metal tags to the environment. The reflection spectra to the port (S_{11} parameters) were numerically calculated for the free-space scenario and for the on-metal tag (a 40 cm × 40 cm metal sheet was considered for the assessment). The matching conditions and the operating frequency were optimized for on-metal performance. Fig. 4 summarizes the results, showing a 13 MHz spectral shift between the matchings for free-space and on-metal cases. The realized gain is a crucial factor: it is $G_t = 0.7$ (linear scale) for the tag in free space and $G_t = 3.1$ for the tag placed on the 40 cm × 40 cm metal sheet. The gain is increased by a factor of 4 owing to the interaction with the metal surface. Increase of the tag's gain implies increasing the RFID reading range. According to the Friis equation [31],

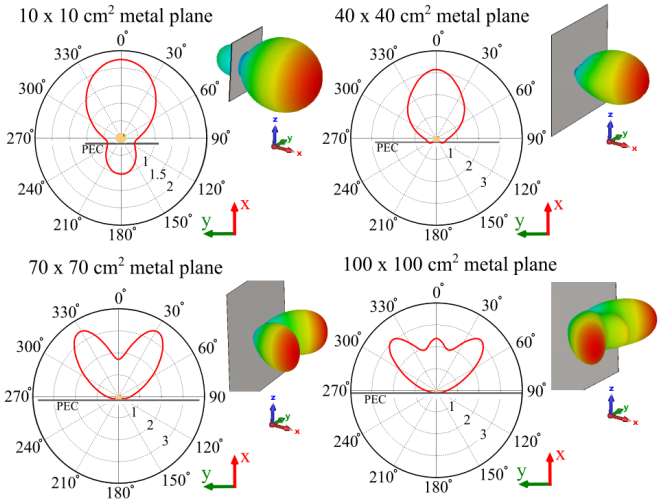

Fig. 5. Polar plots of the radiation pattern (realized gain parameter) in linear scale for different sizes of the metal ground plane. Three-dimensional pattern of the realized gain (in linear scale) (inset).

the reading range (L) should be increased twice

$$L = \frac{\lambda}{4\pi}\sqrt{\frac{P_t G_{TR} G_t}{P_{ch}}} \tag{2}$$

where P_t is the power transmitted by the reader, G_{TR} is the gain of the reader Tx/Rx antenna, G_t is the realized gain of the tag's antenna, P_{ch} is the IC's sensitivity, and λ is the operational wavelength. Based on the numerically calculated parameters, the chip sensitivity from the data sheet, and the custom-made reader's antenna gain $G_{TR} = 7.5$ dBi, the estimated reading range becomes $L = 30.2$ m.

Next, we will study the radiation patterns of on-metal tags tailored by metal substrate. Fig. 5 demonstrates the tag gain in polar coordinates, calculated for different sizes of the metal screen. The differences in the radiation patterns result from edge diffractions and reflections affecting the antenna performance. However, in all the considered cases, the gain in the direction along the surface normal is not lower than 1.85 in the linear scale. Furthermore, the beam is quite wide, covering the 70°–100° spatial sector, which makes the interrogation procedure less sensitive to alignment issues. Following (2), the reading range should not be lower than 20 m in any case. Fig. 5 shows the 3-D pattern of the realized gain (in linear scale) (inset). In several cases, side lobes appear due to interaction with the screen edges.

Fig. 6(a) summarizes the gain as a function of the metal screen size. Gain for an infinite substrate was calculated separately, and it is slightly lower than that of finite-size structures. While the predicted gain of the 10 cm × 10 cm sample resembles the infinite plane performance, it was not considered in the experiment, because it is comparable to the wavelength and, as a result, sensitive to environmental noise.

Finally, the distance between the resonator and the metal surface (40 cm × 40 cm) was investigated parametrically. Fig. 6(b) and (c) shows the radiation efficiency and complex impedance of the tag antenna as functions of the length of

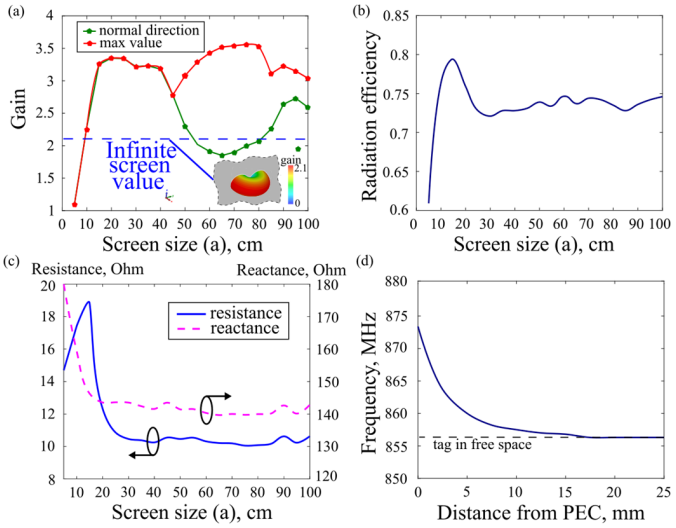

Fig. 6. (a) Tag's antenna gain as a function of the ground plane size is indicated with red line. Green line indicates the gain in the direction normal to the ground plane; the red line is the maximum gain value. The blue line is the gain above an infinite plane. Realized antenna gain in case of an infinite substrate (inset). (b) Radiation efficiency as a function of the ground plane size. (c) Antenna's impedance as a function of the ground plane size. (d) Resonant frequency as a function of the distance between the tag and the 40 cm × 40 cm metal plane.

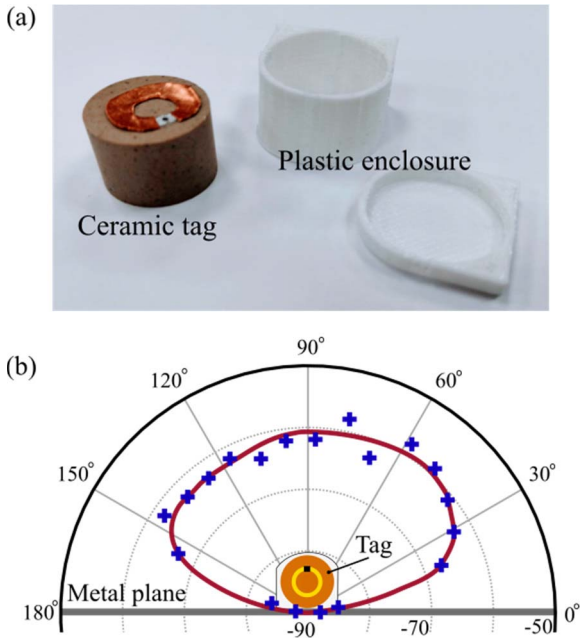

Fig. 7. (a) Photograph of the fabricated on-metal ceramic tag. (b) Measured received signal intensity from the tag (both up and downlinks involved) for different mutual orientations between the tag and the reader.

the side of the metal screen. The structure is quite sensitive to resonant effects when this length is less than 30 cm. However, this effect disappears for lengths larger than the operational wavelength. Fig. 6(d) demonstrates the resonance frequency of the magnetic dipole mode TE_{010} as a function of the tag's distance from the screen. If the tag is located at a distance larger than 15 mm from the screen, the resonance frequency reaches that of the free-space scenario, and the metal screen does not play a role anymore. This behavior is evidence of a strong mode confinement in the high-index ceramic resonator.

III. Experimental Results

After the parametric studies and optimization, we experimentally verified the concept. The dimensions of the fabricated structure are the same as those used in the numerical analysis. Briefly, a nonresonant copper ring with an RFID chip Impinj Monza R6 was placed on the top of a ceramic resonator with radius $R = 7.3$ mm, height $h = 11$ mm, and permittivity $\varepsilon_r = 506$ with $tan\,\delta = 4 \cdot 10^{-4}$ [see Fig. 7(a)]. The structure was placed in a protective plastic enclosure made of a 3-D printed ABS plastic (Raise3-D Pro2 printer was used).

An RFID reader [Impinj R2000, operating at a European standard frequency (865–868 MHz) and radiation power of 27 dBm] was used to interrogate the tag and measure its radiation pattern. A linearly polarized (parallel to the earth surface) custom-made Yagi-Uda antenna with a gain of 7.5 dB was connected to the reader. The reader displays the received signal intensity, which is the function of the mutual orientation between the tag and the reader's antenna. In this type of experiment, both down (tag's excitation) and up (time-modulated backscattered signal) links should be considered. The distance between the reader's antenna and the tag was 1.5 m, which approaches the far-field conditions. A rotary table was used to change the angle in the azimuthal plane between the reader's antenna and the tag attached to the 40 cm × 40 cm metal screen. The amplitude of the received signal was measured with an angular step of 10°. The results are shown in Fig. 7(b).

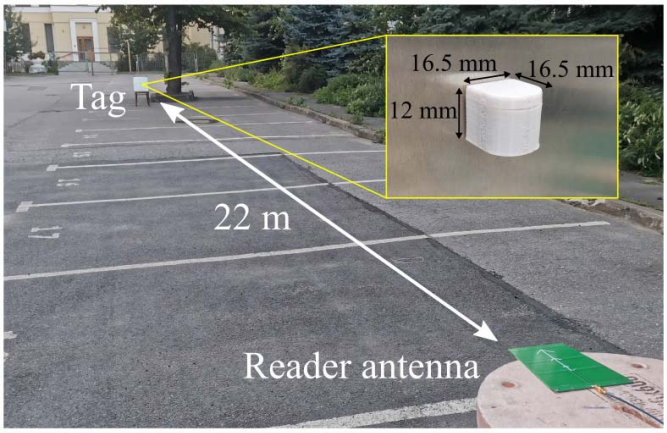

Fig. 8. Photograph of read range measurement. Tag's view in the holder (inset).

At the next stage, we integrated the long-range interrogation. The theoretical prediction was 30 m. The same reader device and Yagi-Uda antenna were used. The effective isotropic radiated power (EIRP) was 2.82 W (34.5 dBm). Fig. 8 shows the experimental setup for determining the maximum reading distance of the tag in an open space. The maximum reading range of the tag, mounted on the 40 cm × 40 cm metal sheet, was found to be 22 m. This value is below the theoretical estimate owing to the outdoors environmental fluctuations.

TABLE III
COMPARING THE PERFORMANCES OF THE METAL-MOUNTABLE RFID TAGS

Ref.	EIRP (W)	Tag dimensions (mm^3)	Chip sensitivity (dBm)	Gain (dB)	Backing plate size (cm^2)	Reading range (m)
This work	2.82	16.5 × 16.5 × 12	-20	3.1	40 × 40	22
[17]	4	176 × 61 × 31	-18	5.9	100 × 100	15
[32]	4	120 × 60 × 0.4	-18	8.7	30 × 15	10
[21]	4	30 × 50 × 3.35	-17.8	-2.5	20 × 20	9.8
[33]	4	64 × 64 × 2	-17	0.3	20 × 20	10.2
[34]	4	71 × 25.5 × 3.2	-14	NA	20 × 20	8.9
[5]	4	104 × 31 × 7.6	-18.5	2.1	30 × 25	14.6
[18]	4	140 × 60 × 10	-20.5	6.43	NA	26
[35]	4	100 × 60 × 10	-14	NA	NA	12.2
[13]	4	25 × 40 × 3	-17.8	-2.23	20 × 20	10.7
[14]	4	60 × 60 × 3	-20	2	20 × 20	22.4
[36]	4	30 × 30 × 2.6	-22.9	NA	22 × 22	6.4
[37]	4	20 × 18 × 1.7	-17.8	2.25	20 × 20	6.5
[38]	4	40 × 5 × 3.2	-20	-3	20 × 20	11
[22]	4	72 × 32 × 6.8	-16	1.79	30 × 30	12.3
[39]	4	29.8×29.8 ×0.813	-22	-9.96	10 × 10	3.6

Finally, we assessed the performance of the new on-metal tag versus other demonstrated designs. We compared our tag with long-range UHF RFID tags for on-metal applications. Table III summarizes the results. Being the most compact in size, our architecture provides a reading range of over 20 m, which can be qualified as the state-of-the-art RFID tag in the footprint-to-reading range ratio. The drawbacks of our realization are its volumetric nature and possible manufacturing costs, though the latter are hard to estimate straightforwardly based on the cost of ICs and ceramic powders.

IV. CONCLUSION

A compact long-range on-metal ceramic tag was demonstrated. The design is based on a compact high-index ceramic resonator and an inductively coupled small metal ring functionalized with an RFID IC. Specifically, 16.5 mm × 16.5 mm × 12 mm footprint device, placed on a 40 cm × 40 cm metal sheet, was successfully interrogated from 22 m without violating the international EIRP standards. To the best of our knowledge, it is the smallest RFID tag on metal with a reading range of over 20 m. The proposed architecture combines three essential functions: small footprint, long reading range, and capability of on-metal labeling, which make this design attractive for numerous possible applications, including the IoST and many others.

ACKNOWLEDGMENT

The authors would like to thank Dr. Elena Bazanova and Lydia Pogorelskaya for critical reading of the manuscript and useful suggestions. They would also like to thank Stanislav Glybovski, Rustam Balafendiev, and Dmitry Zhirihin for useful discussions.

REFERENCES

[1] K. Finkenzeller, *RFID Handbook: Radio-Frequency Identification Fundamentals and Applications*, 2nd ed. New York, NY, USA: Wiley, 2004.
[2] Y.-F. Lin, S.-A. Yeh, H.-M. Chen, and S.-W. Chang, "Design of an omnidirectional polarized RFID tag antenna for safety glass applications," *IEEE Trans. Antennas Propag.*, vol. 60, no. 10, pp. 4530–4537, Oct. 2011.
[3] S.-R. Lee, W.-H. Ng, E.-H. Lim, F.-L. Bong, and B.-K. Chung, "Compact magnetic loop antenna for omnidirectional on-metal UHF tag design," *IEEE Trans. Antennas Propag.*, vol. 68, no. 2, pp. 765–772, Feb. 2020.
[4] H.-D. Chen, C.-H. Tsai, C.-Y.-D. Sim, and C.-Y. Kuo, "Circularly polarized loop tag antenna for long reading range RFID applications," *IEEE Antennas Wireless Propag. Lett.*, vol. 12, pp. 1460–1463, 2013.
[5] A. Hamani, M. C. E. Yagoub, T.-P. Vuong, and R. Touhami, "A novel broadband antenna design for UHF RFID tags on metallic surface environments," *IEEE Antennas Wireless Propag. Lett.*, vol. 16, pp. 91–94, 2017.
[6] A. Mikhailovskaya *et al.*, "Omnidirectional miniature RFID tag," *Appl. Phys. Lett.*, vol. 119, no. 3, Jul. 2021, Art. no. 033503.
[7] S. Krasikov *et al.*, "Multipolar engineering of subwavelength dielectric particles for scattering enhancement," *Phys. Rev. Appl.*, vol. 15, no. 2, Feb. 2021, Art. no. 024052.
[8] D. Dobrykh *et al.*, "Long-range miniaturized ceramic RFID tags," *IEEE Trans. Antennas Propag.*, vol. 69, no. 6, pp. 3125–3131, Jun. 2021.
[9] D. Dobrykh *et al.*, "Multipole engineering for enhanced backscattering modulation," *Phys. Rev. B, Condens. Matter*, vol. 102, no. 19, Nov. 2020, Art. no. 195129.
[10] K. V. S. Rao, S. F. Lam, and P. V. Nikitin, "UHF RFID tag for metal containers," in *Proc. Asia–Pacific Microw. Conf. (APMC)*, Dec. 2010, pp. 179–182.
[11] A. Buffi and P. Nepa, "An RFID-based technique for train localization with passive tags," in *Proc. IEEE Int. Conf. RFID (RFID)*, May 2017, pp. 155–160.
[12] A. A. Babar, T. Bjorninen, V. A. Bhagavati, L. Sydanheimo, P. Kallio, and L. Ukkonen, "Small and flexible metal mountable passive UHF RFID tag on high-dielectric polymer-ceramic composite substrate," *IEEE IEEE Antennas Wireless Propag. Lett.*, vol. 11, pp. 1319–1322, 2012.
[13] C.-W. Moh, E.-H. Lim, F.-L. Bong, and B.-K. Chung, "Miniature coplanar-fed folded patch for metal mountable UHF RFID tag," *IEEE Trans. Antennas Propag.*, vol. 66, no. 5, pp. 2245–2253, May 2018.
[14] P. Wang, W. Luo, Y. Shao, and H. Jin, "An UHF RFID circularly polarized tag antenna with long read distance for metal objects," *IEEE Antennas Wireless Propag. Lett.*, vol. 21, no. 2, pp. 217–221, Feb. 2022.
[15] H.-D. Chen and Y.-H. Tsao, "Low-profile meandered patch antennas for RFID tags mountable on metallic objects," *IEEE Antennas Wireless Propag. Lett.*, vol. 9, pp. 118–121, 2010.
[16] W. Choi, H. W. Son, J.-H. Bae, G. Y. Choi, C. S. Pyo, and J.-S. Chae, "An RFID tag using a planar Inverted-F antenna capable of being stuck to metallic objects," *ETRI J.*, vol. 28, no. 2, pp. 216–218, Apr. 2006.
[17] K. Hwan Lee *et al.*, "Design of a UHF RFID metal tag for long reading range using a cavity structure," in *Proc. Asia–Pacific Microw. Conf. (APMC)*, Dec. 2008, pp. 1–4.
[18] F. K. Byondi and Y. Chung, "Longest-range UHF RFID sensor tag antenna for IoT applied for metal and non-metal objects," *Sensors*, vol. 19, no. 24, p. 5460, Dec. 2019.
[19] R. S. Elliott, *Antenna Theory and Design*, vol. 23, no. 5. Hoboken, NJ, USA: Wiley, 2003.
[20] C. E. Balanis, *Antenna Theory: Analysis and Design*, 3rd ed., C. A. Balanis, Ed. Hoboken, NJ, USA: Wiley, 2005, p. 1136.

[21] N. Ripin, E.-H. Lim, F.-L. Bong, and B.-K. Chung, "Miniature folded dipolar patch with embedded AMC for metal mountable tag design," *IEEE Trans. Antennas Propag.*, vol. 68, no. 5, pp. 3525–3533, May 2020.
[22] X. Li, G. Gao, H. Zhu, Q. Li, N. Zhang, and Z. G. Qi, "UHF RFID tag antenna based on the DLS-EBG structure for metallic objects," *IET Microw., Antennas Propag.*, vol. 14, no. 7, pp. 567–572, Mar. 2020.
[23] E. A. Nenasheva *et al.*, "Low loss microwave ferroelectric ceramics for high power tunable devices," *J. Eur. Ceram. Soc.*, vol. 30, no. 2, pp. 395–400, Jan. 2010.
[24] D. Dobrykh, I. Yusupov, P. Ginzburg, A. Slobozhanyuk, and D. Filonov, "Self-aligning roly-poly RFID tag," *Sci. Rep.*, vol. 12, no. 1, pp. 1–7, Feb. 2022.
[25] R. F. Harrington, *Time-Harmonic Electromagnetic Fields*, 2nd ed. New York, NY, USA: Wiley, 2001.
[26] S. Kosulnikov, D. Filonov, A. Boag, and P. Ginzburg, "Volumetric metamaterials versus impedance surfaces in scattering applications," *Sci. Rep.*, vol. 11, no. 1, p. 9571, May 2021.
[27] D. Vovchuk, S. Kosulnikov, R. E. Noskov, and P. Ginzburg, "Wire resonator as a broadband Huygens superscatterer," *Phys. Rev. B, Condens. Matter*, vol. 102, no. 9, Sep. 2020, Art. no. 094304.
[28] G. D. Vendelin, A. M. Pavio, and U. L. Rohde, *Microwave Circuit Design Using Linear and Nonlinear Techniques*. Hoboken, NJ, USA: Wiley, 2005.
[29] W.-H. Ng, E.-H. Lim, F.-L. Bong, and B.-K. Chung, "Folded patch antenna with tunable inductive slots and stubs for UHF tag design," *IEEE Trans. Antennas Propag.*, vol. 66, no. 6, pp. 2799–2806, Jun. 2018.
[30] D. M. Pozar, *Microwave Engineering*, 4th ed. Hoboken, NJ, USA: Wiley, 2011.
[31] P. V. Nikitin and K. V. S. Rao, "Theory and measurement of backscattering from RFID tags," *IEEE Antennas Propag. Mag.*, vol. 48, no. 6, pp. 212–218, Dec. 2006.
[32] Y. F. Lin, M. J. Chang, H. M. Chen, and B. Y. Lai, "Gain enhancement of ground radiation antenna for RFID tag mounted on metallic plane," *IEEE Trans. Antennas Propag.*, vol. 64, no. 4, pp. 1193–1200, Apr. 2016.
[33] E.-S. Yang and H.-W. Son, "Dual-polarised metal-mountable UHF RFID tag antenna for polarisation diversity," *Electron. Lett.*, vol. 52, no. 7, pp. 496–498, Apr. 2016.
[34] H.-W. Son and S.-H. Jeong, "Wideband RFID tag antenna for metallic surfaces using proximity-coupled feed," *IEEE Antennas Wireless Propag. Lett.*, vol. 10, pp. 377–380, 2011.
[35] I.-Y. Park and D. Kim, "Artificial magnetic conductor loaded long-range passive RFID tag antenna mountable on metallic objects," *Electron. Lett.*, vol. 50, no. 5, pp. 335–336, Feb. 2014.
[36] N. M. Tan, Y.-F. Lin, C.-H. Chang, C.-T. Liao, and H.-M. Chen, "Compact shorted C-shaped patch antenna for UHF RFID tag mounted on metallic objects," in *Proc. Int. Workshop Electromagn., Appl. Student Innov. Competition (iWEM)*, Aug. 2020, pp. 1–2.
[37] Y.-H. Niew, K.-Y. Lee, E.-H. Lim, F.-L. Bong, and B.-K. Chung, "Miniature dipolar patch antenna with nonresonating ring for metal-insensitive UHF RFID tag design," *IEEE Trans. Antennas Propag.*, vol. 68, no. 3, pp. 2393–2398, Mar. 2020.
[38] K. Thirappa, E.-H. Lim, F.-L. Bong, and B.-K. Chung, "Slim RFID tag antenna for metallic tools with narrow footprint," *IEEE J. Radio Freq. Identificat.*, vol. 5, no. 2, pp. 182–190, Jun. 2021.
[39] D. Inserra and G. Wen, "Low profile metal tolerant UHF RFID tag with lumped elements for post-manufacturing frequency tuning," *IEEE Trans. Antennas Propag.*, vol. 69, no. 11, pp. 7953–7958, Nov. 2021.

Ildar Yusupov (Member, IEEE) was born in Petropavlovsk, Kazakhstan, in 1996. He received the M.S. degree in radiophysics from ITMO University, Saint Petersburg, Russia, in 2020, where he is currently pursuing the Ph.D. degree with the School of Physics and Engineering.

His current research interests include microwave devices, radio frequency identification (RFID), and metamaterials.

Dmitry Dobrykh (Graduate Student Member, IEEE) was born in Perm, Russia, in 1995. He received the M.Sc. degree in radiophysics from ITMO University, Saint Petersburg, Russia, in 2019. He is currently pursuing the Ph.D. degree with the School of Electrical Engineering, Tel Aviv University, Tel Aviv, Israel.

His current research interests include antennas and microwave devices, radio frequency identification (RFID), metamaterials, and topological photonics.

Dmitry Filonov (Member, IEEE) was born in Saint Petersburg, Russia, in 1991. He received the B.Sc. and M.Sc. degrees in photonics from ITMO University, Saint Petersburg, in 2013 and 2015, respectively, and the Ph.D. degree from Tel Aviv University, Tel Aviv, Israel, in 2019.

He is currently the Head of the Radiophotonics Laboratory and an Assistant Professor with the Moscow Institute of Physics and Technology, Moscow, Russia. His main research interests include antenna, applied electromagnetics, all-dielectric structures, radio frequency identification (RFID), and metamaterials.

Alexey Slobozhanyuk (Member, IEEE) was born in Saint Petersburg, Russia, in 1991. He received the B.Sc. and M.Sc. degrees in photonics from ITMO University, Saint Petersburg, Russia, in 2013 and 2015, respectively, and the Ph.D. degree from Australian National University, Canberra, ACT, Australia.

He is currently an Assistant Professor with ITMO University. His main research interests include applied electromagnetics, metamaterials, photonic topological insulators, and metasurfaces.

Pavel Ginzburg (Member, IEEE) received the Ph.D. degree from Technion, Haifa, Israel, in 2011.

He is currently an Associated Professor with Tel Aviv University, Tel Aviv, Israel. He is also the Head of the "Dynamics of Nanostructures" Laboratory, encompassing theoretical group, optical spectroscopy, and radio waves labs. The laboratory runs multidisciplinary research in the field of bio photonics quantum mechanics, nano-plasmonics and metamaterials, optical forces, and radio physics.

Dr. Ginzburg is also the former EPSRC Research Fellow, the International Newton Research Fellow, and the Rothschild Fellow with King's College London.